

Cardiovascular Shunts: MR Imaging Evaluation¹

Zhen J. Wang, MD • Gautham P. Reddy, MD, MPH • Michael B. Gotway, MD • Benjamin M. Yeh, MD • Charles B. Higgins, MD

Magnetic resonance (MR) imaging has become an important tool for the accurate and noninvasive assessment of congenital heart disease. Because more precise delineation of anatomy and evaluation of function can be obtained with MR imaging than with either echocardiography or angiography, MR imaging is frequently used to evaluate cardiovascular shunt lesions. It is essential that imaging specialists be able to recognize the MR imaging features of various kinds of shunts, including supracristal ventricular septal defect, atrioventricular septal defect, and partial anomalous pulmonary venous connection. MR imaging is particularly useful for evaluating shunt severity, which can be expressed quantitatively as the ratio of pulmonary flow to systemic flow. This ratio can be estimated accurately with the use of either volumetric cine MR imaging or velocity-encoded cine MR imaging.

©RSNA, 2003

Abbreviation: PAPVR = partial anomalous pulmonary venous return

Index terms: Heart, flow dynamics, 50.12144 • Heart, function • Heart, MR, 50.1214 • Magnetic resonance (MR), cine study • MR, vascular studies

RadioGraphics 2003; 23:S181–S194 • Published online 10.1148/rg.23si035503

¹From the Department of Radiology, Box 0628, University of California, 505 Parnassus Ave, San Francisco, CA 94143-0628. Recipient of a Certificate of Merit award for an education exhibit at the 2002 RSNA scientific assembly. Received February 3, 2003; revision requested March 20 and received May 1; accepted May 20. **Address correspondence to** G.P.R. (e-mail: gautham.reddy@radiology.ucsf.edu).

©RSNA, 2003

Table 1
Uses of MR Imaging in the Anatomic Diagnosis and Functional Evaluation of Cardiovascular Shunts

Shunt Type	Use for Anatomic Diagnosis*	Use for Functional Evaluation†
Atrial septal defect	Adjunct to echocardiography	Shunt quantification
Ventricular septal defect	Adjunct to echocardiography (in supracristal ventricular septal defect, preferred over echocardiography and conventional angiography)	Shunt quantification
Atrioventricular septal defect	Preferred over echocardiography and conventional angiography	NA
Patent ductus arteriosus	Adjunct to echocardiography	Shunt quantification
Aortopulmonary window	Adjunct to echocardiography	Shunt quantification
PAPVR	Preferred over echocardiography and conventional angiography	Shunt quantification

*Standard MR imaging and MR angiographic techniques are used for diagnostic evaluation.

†Volumetric or velocity-encoded cine MR imaging techniques may be used for functional evaluation except in ventricular septal defect, in which only velocity encoding may be used to quantify shunt volume. NA = not applicable.

Introduction

Magnetic resonance (MR) imaging has become an important tool for the delineation of cardiac anatomy and the quantification of physiologic function (1–7). It has multiple capabilities for the evaluation of congenital heart diseases including cardiovascular shunts. Morphologic information about shunts is provided by electrocardiography (ECG)-gated spin-echo and cine MR imaging. Shunt volume can be estimated by using volumetric cine MR imaging or velocity-encoded cine MR imaging. MR angiography permits high-resolution three-dimensional examination of vessels and can noninvasively establish the presence of anomalous pulmonary veins that lead to shunting (8,9).

Echocardiography and angiography have traditionally been the primary imaging modalities used for the evaluation of cardiac shunts. Echocardiography is sensitive and noninvasive but has a limited acoustic window. Although angiography is frequently considered the standard method for achieving definitive diagnosis of cardiac shunts, it is invasive and requires the use of iodinated contrast material. Computed tomography (CT) can demonstrate structural heart disease such as septal defects and anomalous pulmonary venous and arterial anatomy; however, functional evaluation of shunts with CT has not been described extensively. MR imaging has emerged as an accurate and noninvasive alternative for the depiction of anatomy and the assessment of function. This article surveys the MR imaging techniques that are most useful for detecting, localizing, and

Table 2
Optimal MR Imaging Planes for the Depiction of Cardiovascular Shunts

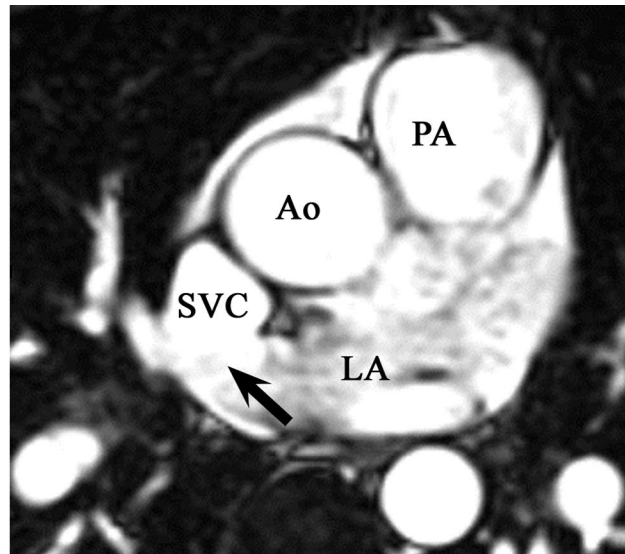
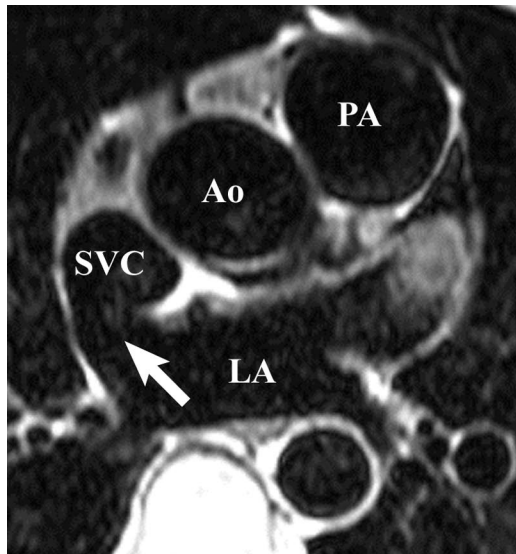
Shunt Type	Optimal MR Imaging Plane
Atrial septal defect	Axial
Ventricular septal defect	Axial or coronal
Atrioventricular septal defect	Axial
Patent ductus arteriosus	Sagittal oblique
Aortopulmonary window	Axial or coronal
PAPVR	Coronal

quantifying shunts in atrial, ventricular, and atrioventricular septal defects; patent ductus arteriosus; aortopulmonary window; and partial anomalous pulmonary venous return (PAPVR) (Tables 1, 2).

Atrial Septal Defect

Atrial septal defect is the most common shunt lesion detected de novo in adulthood (10). It accounts for at least 30% of all congenital cardiac defects in individuals older than 40 years (11). Although adolescents and young adults with a defect of the septum secundum are commonly asymptomatic, more than half will develop dyspnea, easy fatigability, atrial flutter or fibrillation, right heart failure, or pulmonary hypertension by age 40 (12).

The sinus venosus and the septa secundum and primum can be clearly visualized with MR imaging in the transverse plane or along the short axis. Spin-echo MR imaging has been found accurate for the detection and localization of atrial septal defect with greater than 90% sensitivity and specificity (13). MR imaging criteria used to



a.

b.

Figure 1. Sinus venous atrial septal defect in a 50-year-old woman with dyspnea on exertion. Axial ECG-gated spin-echo (**a**) and cine (**b**) MR images show a defect (arrow) in the portion of the atrial septum between the superior vena cava (SVC) and the left atrium (LA). Ao = ascending aorta, PA = main pulmonary artery.

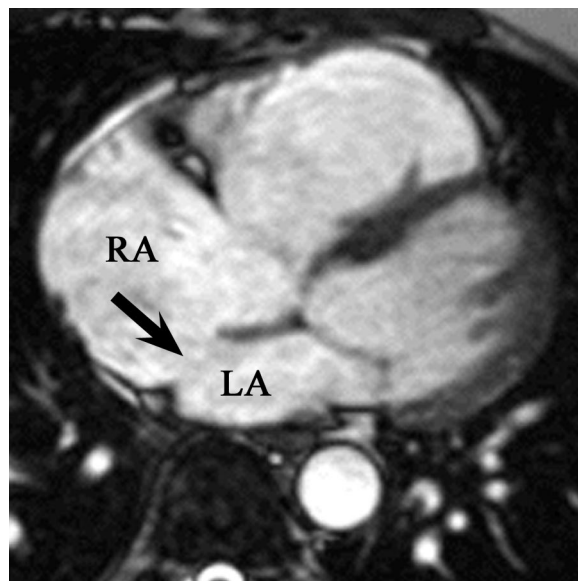
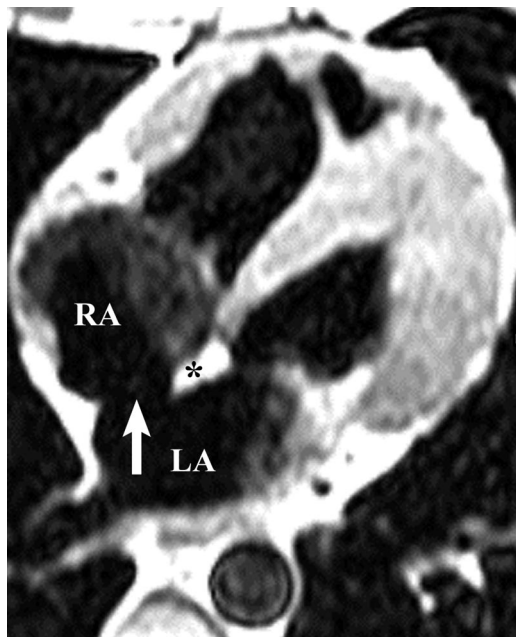


Figure 2. Atrial septal defect in the septum secundum in a 23-year-old man with a heart murmur. Axial ECG-gated spin-echo image shows a defect (arrow) in the middle of the septum and thickening (*) at the edge of the septum adjacent to the defect. LA = left atrium, RA = right atrium.

Figure 3. Atrial septal defect in the septum secundum in a 45-year-old man with dyspnea on exertion. Axial ECG-gated cine MR image shows a defect (arrow) in the middle of the atrial septum. LA = left atrium, RA = right atrium.

establish the presence of atrial septal defect include depiction of the defect at two adjacent anatomic levels on multisection transverse images or at the same anatomic level on single-section images acquired during multiple phases of the cardiac cycle (14). MR images of patients with an

atrial septal defect involving the sinus venosus show a defect in the portion of the atrial septum between the superior vena cava and the left atrium (Fig 1). In patients with a defect of the septum secundum, the defect occurs in the middle of the atrial septum (Figs 2, 3). The normally thinned tissue in the region of the fossa ovalis, which may exhibit little or no signal intensity

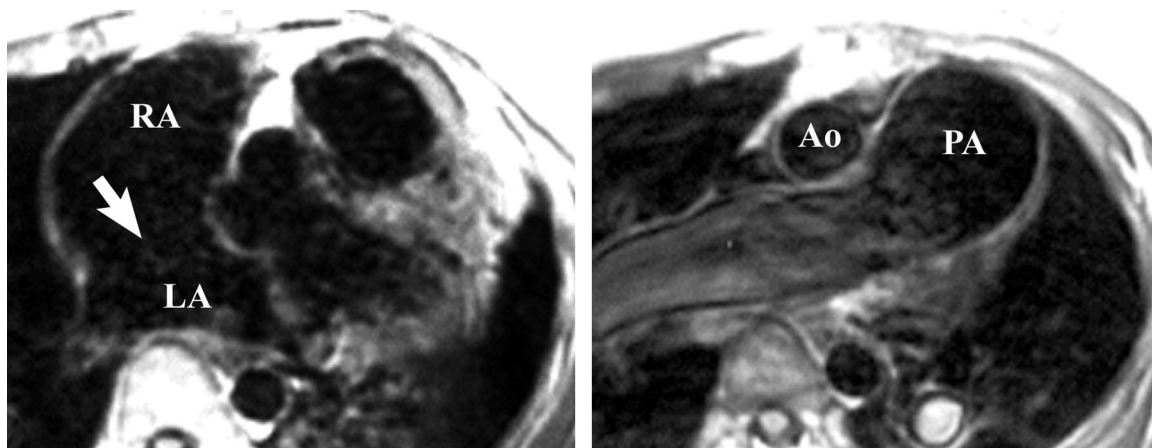


Figure 5. Eisenmenger syndrome in a 36-year-old woman. Axial ECG-gated spin-echo images show atrial septal defect (arrow in **a**) and marked enlargement of the main pulmonary artery (*PA*) (**b**), consistent with pulmonary arterial hypertension. Long-standing severe pulmonary arterial hypertension can result in the shunt reversal that characterizes Eisenmenger syndrome. *Ao* = ascending aorta, *LA* = left atrium, *RA* = right atrium.

on MR images, is sometimes mistaken for a defect in the septum secundum (Fig 4). An intact atrial septum, however, thins gradually toward the site of signal intensity absence (Fig 4). In contrast, in a defect of the septum secundum, the edge of the adjacent septum is thickened (Figs 2, 3). A defect of the septum primum is frequently associated with a defect of the atrioventricular valve (atrioventricular septal defect). The use of MR imaging for the evaluation of atrioventricular septal defect is described later in this article.

Currently, echocardiography is the primary imaging modality used in the evaluation of atrial septal defects, because of its high sensitivity and specificity, low cost, and accessibility. However, MR imaging has several distinct advantages over echocardiography. Phase-contrast cine MR imaging enables more precise evaluation of the size and shape of atrial septal defects, as well as quantification of the degree of shunting (15,16). MR imaging also accurately portrays the anatomy of the right ventricle and pulmonary arteries, which is particularly important in patients with long-standing atrial septal defect and pulmonary hypertension (Fig 5).

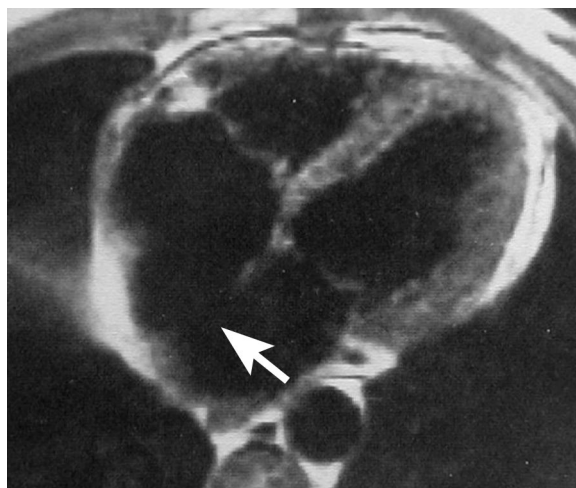
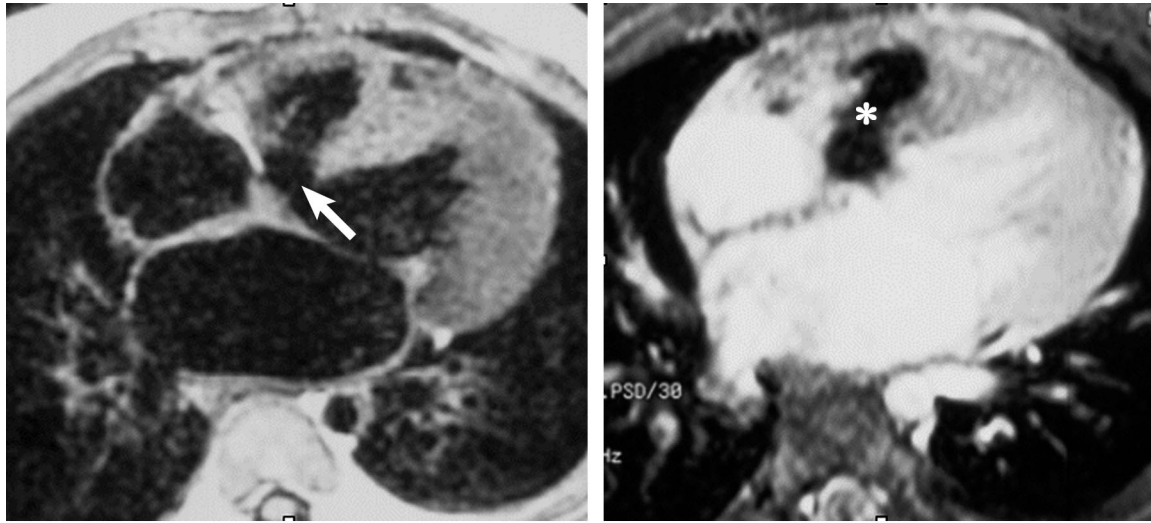


Figure 4. Normal atrial septum. Axial ECG-gated spin-echo image shows little signal intensity in the region of the fossa ovalis, in the interatrial septum (arrow)—a finding that could lead to a false-positive identification of atrial septal defect in the septum secundum.

Ventricular Septal Defect

Ventricular septal defect is the second most common congenital malformation of the heart and accounts for approximately 20% of all congenital



a.

b.

Figure 6. Membranous ventricular septal defect in an 11-month-old boy with a heart murmur. **(a)** Axial ECG-gated spin-echo image shows a defect (arrow) in the membranous part of the septum. **(b)** Axial gradient-echo cine image shows a flow jet (*) across the defect into the right ventricle, indicating a left-to-right shunt.

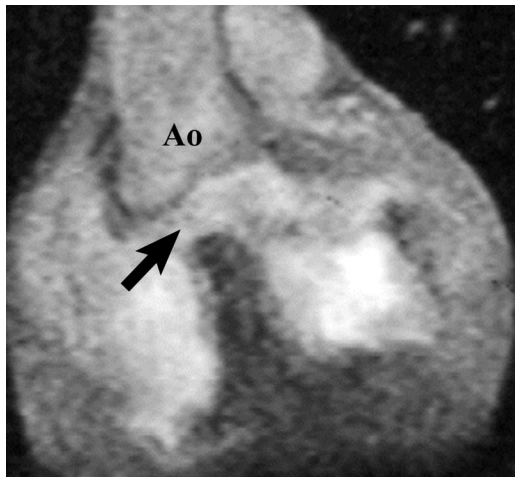
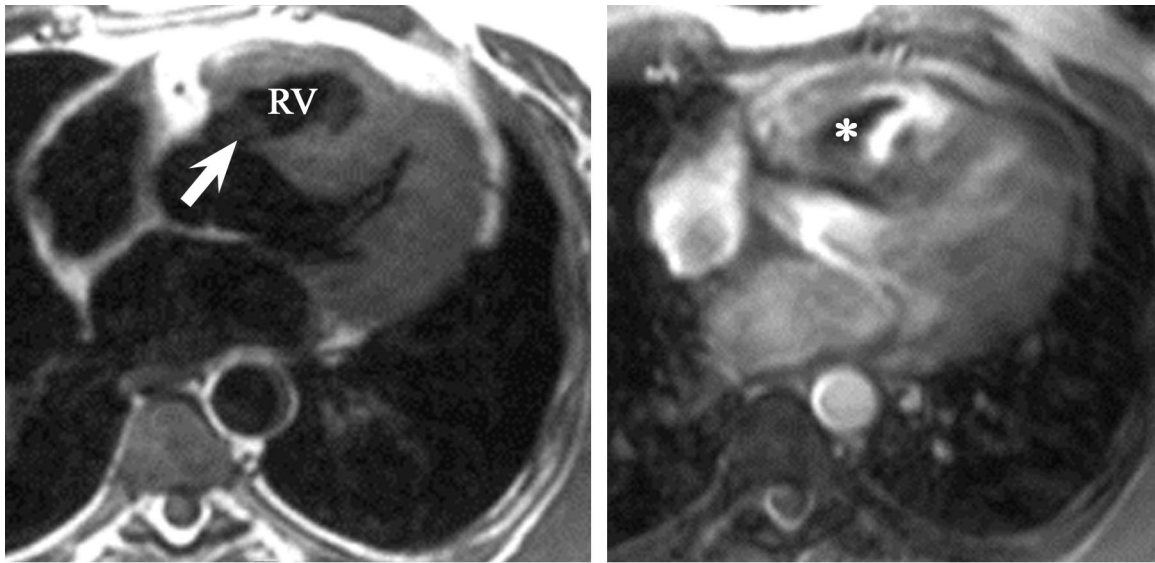


Figure 7. Membranous ventricular septal defect in a 24-year-old man with tetralogy of Fallot. Coronal ECG-gated cine MR image shows a membranous ventricular septal defect (arrow) with an overriding aorta (Ao). (Courtesy of James Scatliff, MD, Department of Radiology, University of North Carolina, Chapel Hill)

cardiac malformations (10). Ventricular septal defects can be classified into four main categories according to their location and margin: outlet,

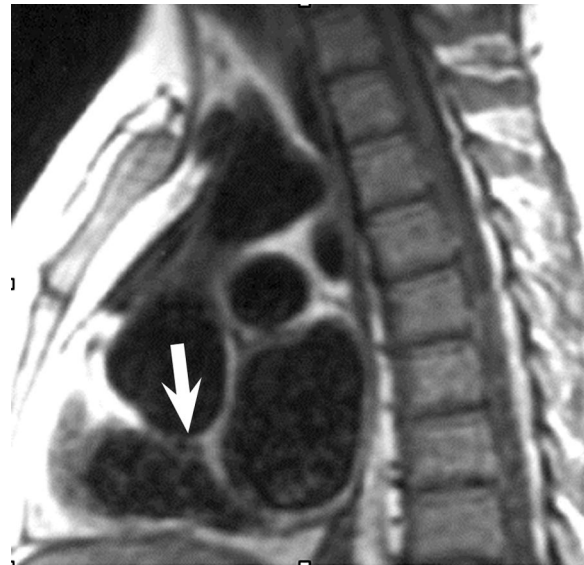
membranous, trabecular, and inlet (17). Defects involving the outlet septum include subpulmonic defects and malalignment defects associated with truncus arteriosus, tetralogy of Fallot, and double-outlet right ventricle. The most frequently encountered ventricular septal defect is of the membranous category (Figs 6, 7). It lies adjacent to the central fibrous skeleton of the heart with the membranous part of the septum as one of its borders. A defect that is contained entirely within the confines of the muscular septum is termed *muscular* or *trabecular* ventricular septal defect. The fourth type of ventricular septal defect involves the inlet septum and is associated with atrioventricular septal defects. Ventricular septal defect also may be described in relation to the crista supraventricularis of the right ventricle; a *supracristal* defect is located above the crista muscle at the ventricular outlet (Fig 8) and appears to connect the right ventricular outflow tract directly to the aorta. This type of ventricular septal defect also has been described as a *doubly committed subarterial* defect because its location is both subaortic and subpulmonary (17).



a.

b.

Figure 8. Supracristal ventricular septal defect in an asymptomatic 42-year-old man with a systolic murmur. (a) Axial ECG-gated spin-echo image shows a defect (arrow) between the base of the aorta and the right ventricular (RV) infundibulum. (b) Axial gradient-echo systolic cine image shows a flow jet (*) from the left ventricle into the right ventricular outflow tract, indicating a left-to-right shunt. (c) Sagittal spin-echo image shows a prolapse (arrow) of the posterior aortic sinus of Valsalva.



c.

Although the diagnosis of ventricular septal defect is usually established by means of echocardiography, other modalities also are used, including MR imaging, angiography, and, occasionally, electron-beam CT or multi-detector row CT (18,19). MR imaging, with a reported sensitivity of more than 90% for detection of ventricular septal defects (20), is an accurate and noninvasive alternative to echocardiography. In particular, MR imaging has advantages over echocardiography and angiography for the diagnosis of supracristal ventricular septal defects (21). Additionally, it plays an important role in the evaluation of ventricular septal defects involving the inlet septum in patients with atrioventricular septal defects.

Supracristal Ventricular Septal Defect

MR imaging plays an important role in the diagnosis and management of supracristal ventricular septal defect. Although echocardiography is the primary imaging modality for the evaluation of cardiac shunts, it is less accurate for defining supracristal ventricular septal defect. Cardiac angiography is more accurate in localizing the

lesion, but it involves catheterization and ionizing radiation, with attendant risks to the patient. MR imaging is an effective and noninvasive alternative (21). ECG-gated spin-echo MR images typically depict a characteristic defect between the base of the aorta and the right ventricular infundibulum (Fig 8a), and cine MR images often reveal a systolic flow jet from the left ventricle into the right ventricular outflow tract, indicating a left-to-right shunt (Fig 8b). Shunt severity can be quantified by calculating the ratio of pulmonary flow to systemic flow, with flow values obtained from velocity-encoded cine MR images (16,22). Furthermore, MR imaging can be used to diagnose complications of supracristal ventricular septal defect, including aortic valve prolapse with resultant aortic regurgitation and secondary right ventricular enlargement or hypertrophy (21) (Fig 8c).

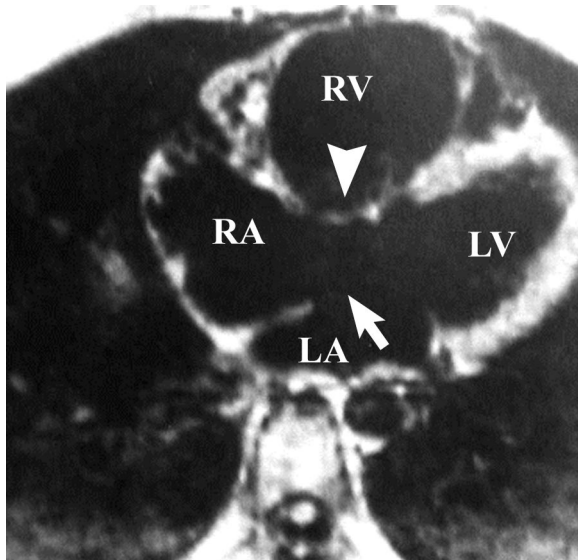


Figure 9. Atrioventricular septal defect. Axial ECG-gated spin-echo image shows an atrial septal defect (arrow) in the septum primum. The atrioventricular valve (arrowhead) is connected with the crest of the inlet ventricular septum. *LA* = left atrium, *LV* = left ventricle, *RA* = right atrium, *RV* = right ventricle.

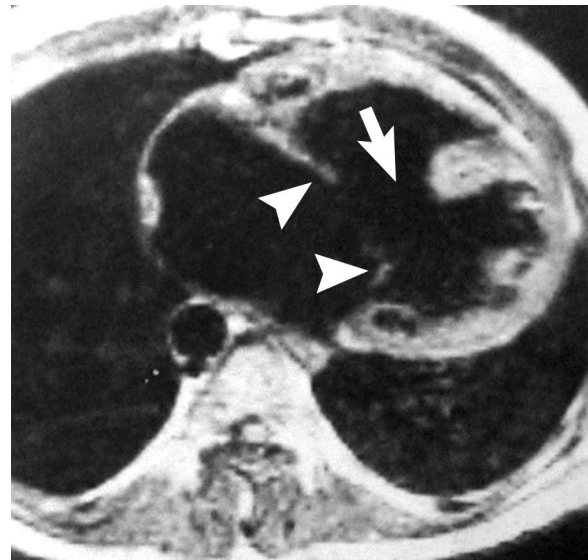
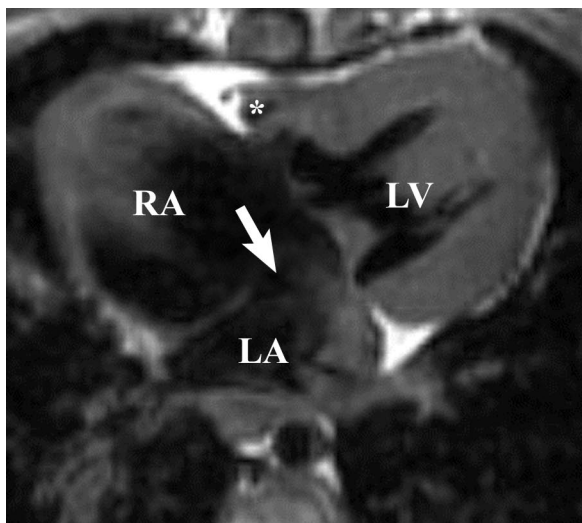
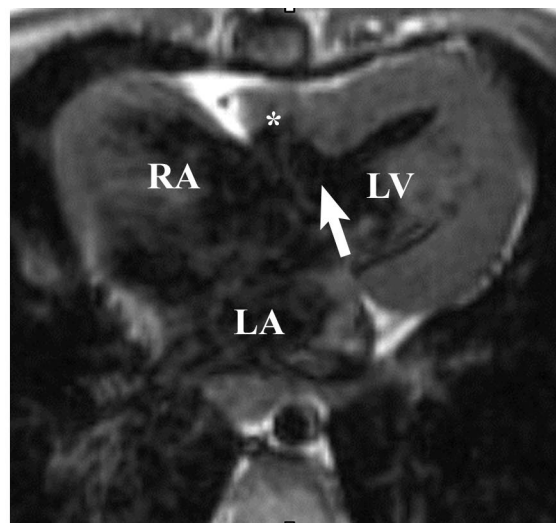


Figure 10. Atrioventricular septal defect. Axial ECG-gated spin-echo image shows a complete atrioventricular septal defect with communication among all four chambers, as well as a large inlet ventricular septal defect (arrow). The single atrioventricular valve (arrowheads) spans both ventricular chambers.



a.



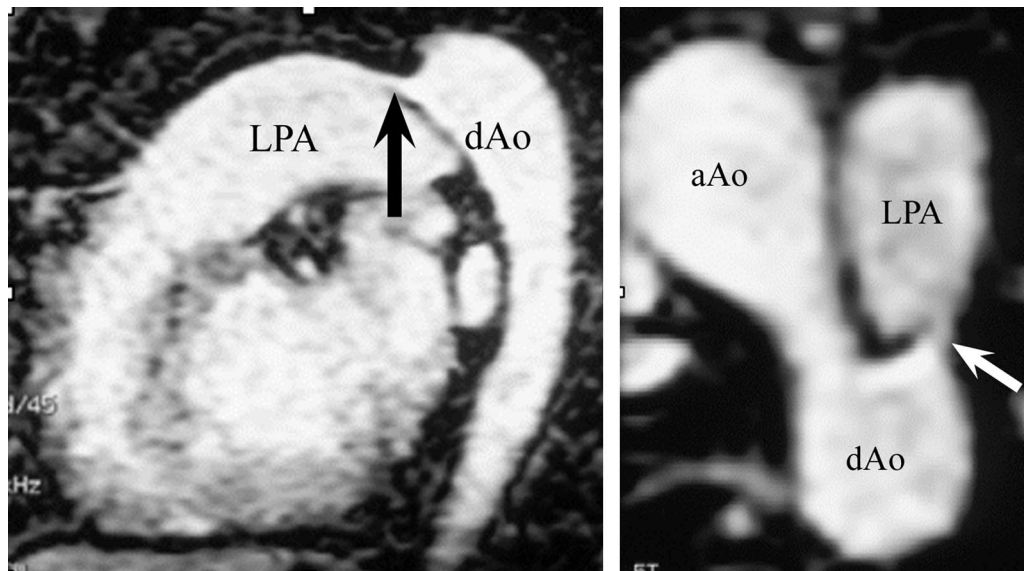
b.

Figure 11. Atrioventricular septal defect in a 2-year-old girl. Axial ECG-gated spin-echo MR images show an atrial septal defect (arrow in **a**) in the septum primum and an inlet ventricular septal defect (arrow in **b**), which together produce communication among all four chambers. The right atrium (*RA*) is markedly enlarged and the right ventricle (*) is hypoplastic. *LA* = left atrium, *LV* = left ventricle.

Atrioventricular Septal Defect

Atrioventricular septal defect, formerly known as endocardial cushion defect, manifests as a common atrioventricular valve with an abnormal arrangement of valvular leaflets and variable deficiency of the atrial septum primum and the ventricular inlet septum (Figs 9–11) (14). Direct shunting from the left ventricle to the right atrium may occur through a defect in the atrioventricular septum, the small part of the ventricular septum

that separates the inlet region of the left ventricle from the right atrium. In the most serious form of atrioventricular septal defect, all four chambers of the heart communicate, resulting in both left-to-right and right-to-left shunting (Figs 10, 11b). Although cyanosis may not be clinically apparent, pulmonary arterial hypertension tends to develop in infancy or early childhood in individuals with



a.
Figure 12. Patent ductus arteriosus in a 46-year-old woman with a heart murmur. **(a)** Gadolinium-enhanced MR angiographic image shows a patent ductus (arrow) connecting the proximal descending aorta (*dAo*) to the left pulmonary artery (*LPA*), just beyond the pulmonary arterial bifurcation. Note the focal dilatation of the aorta at the site of ductal attachment. **(b, c)** Axial **(b)** and oblique **(c)** MR angiographic images also depict the ductus (arrow). *aAo* = ascending aorta. (Courtesy of Ruth Carlos, MD, Department of Radiology, University of Michigan, Ann Arbor)

this form of atrioventricular septal defect. Clinically, the less severe forms resemble atrial septal defect, but the symptoms in atrioventricular septal defect are frequently more severe.

MR imaging is a valuable tool for the evaluation of atrioventricular septal defects, among which there is considerable morphologic variation, and is particularly useful in delineating anatomic features important to surgical planning (23). For example, MR imaging is superior to echocardiography and angiography in depicting the presence and size of the ventricular component of the defect, information that may aid in the timing of surgery (23). Another advantage of MR imaging over echocardiography is its ability to accurately depict cardiac chamber dimensions. This information is important because one determinant of surgical risk in patients with atrioventricular septal defects is the presence of ventricular hypoplasia (24).

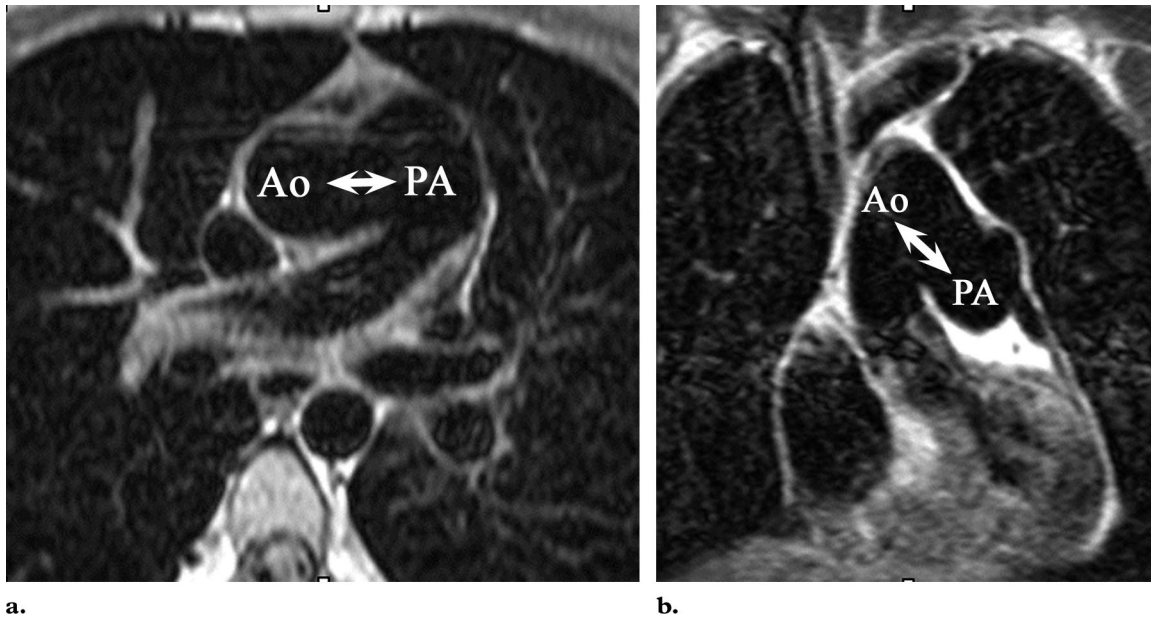


c.

Patent Ductus Arteriosus

Patent ductus arteriosus accounts for approximately 10%–12% of all congenital heart disease (10). Clinical manifestations depend on the size of the duct and the difference between systemic and pulmonary vascular resistance. A small shunt does not cause hemodynamic derangement but may predispose patients to endocarditis; a large shunt causes a progressive increase in pulmonary arterial pressure, which may result eventually in Eisenmenger syndrome.

MR images can clearly depict the connection between the aorta and the pulmonary artery (Fig



a.

b.

Figure 13. Aortopulmonary window in a 20-year-old woman. Axial (a) and coronal (b) ECG-gated spin-echo images show a large defect (double arrow) between the lateral aspect of the ascending aorta (Ao) and the medial aspect of the main pulmonary artery (PA).

12), showing the course of the ductus from the proximal descending aorta to the left pulmonary artery, just beyond the pulmonary arterial bifurcation. MR images also can show focal dilatation of the aorta at the site of ductal attachment (Fig 12a). The large aortic arch that frequently is associated with patent ductus arteriosus also can be seen on MR images. However, a narrow patent ductus may be missed at MR imaging, even with the use of thin (3-mm) sections (14). Echocardiography remains the main diagnostic study used for patent ductus arteriosus. Angiography is used to delineate anatomy and guide coil embolization of the patent ductus arteriosus. Although the accuracy of MR imaging for diagnosis of patent ductus arteriosus is as yet unknown, this modality may be useful for quantifying shunt volume.

Aortopulmonary Window

Aortopulmonary window is a rare congenital heart defect in which the ascending aorta communicates directly with the main pulmonary artery. It differs from truncus arteriosus in that both the aortic and the pulmonary valves are present. Common associated lesions include ventricular septal defect, patent ductus arteriosus, and coarctation of the aorta (14). Patients with this condition typically manifest signs and symptoms of congestive heart failure early in life. Diagnosis is

usually suggested by echocardiographic findings and confirmed with angiography. Although the role of MR imaging in the diagnosis of aortopulmonary window has not been investigated extensively, a number of published reports indicate that MR imaging can fully depict the anatomic features of aortopulmonary window (25,26). Transverse and coronal spin-echo images can depict the abnormal connection between the aorta and the pulmonary trunk (Fig 13), and cine images can reveal a left-to-right shunt. MR images also may be useful for quantifying shunt volume.

Partial Anomalous Pulmonary Venous Return

In PAPVR, one or more pulmonary veins return anomalously to the superior or the inferior vena cava, the right atrium, or the coronary sinus. Drainage of the right pulmonary veins into the inferior vena cava also is known as scimitar syndrome. PAPVR is present in 10%–15% of patients with atrial septal defects of the septum secundum and in nearly 100% of patients with defects involving the sinus venosus (14). Affected children usually remain asymptomatic. Dyspnea and palpitations may occur in older patients.

Figure 14. PAPVR in a 64-year-old woman. (a, b) Axial (a) and coronal (b) ECG-gated spin-echo images show drainage of the right upper lobe pulmonary vein (arrow) into the superior vena cava (SVC). Note the enlarged pulmonary artery (PA) in a, consistent with pulmonary arterial hypertension. (c) Axial spin-echo image at a lower level shows an associated atrial septal defect (arrow) in the sinus venosus. (d) Coronal gadolinium-enhanced MR angiographic image again shows drainage of the right upper lobe pulmonary vein (arrow) into the superior vena cava. The right upper lobe pulmonary vein is the most common anomalous vein. Ao = aorta, LA = left atrium.

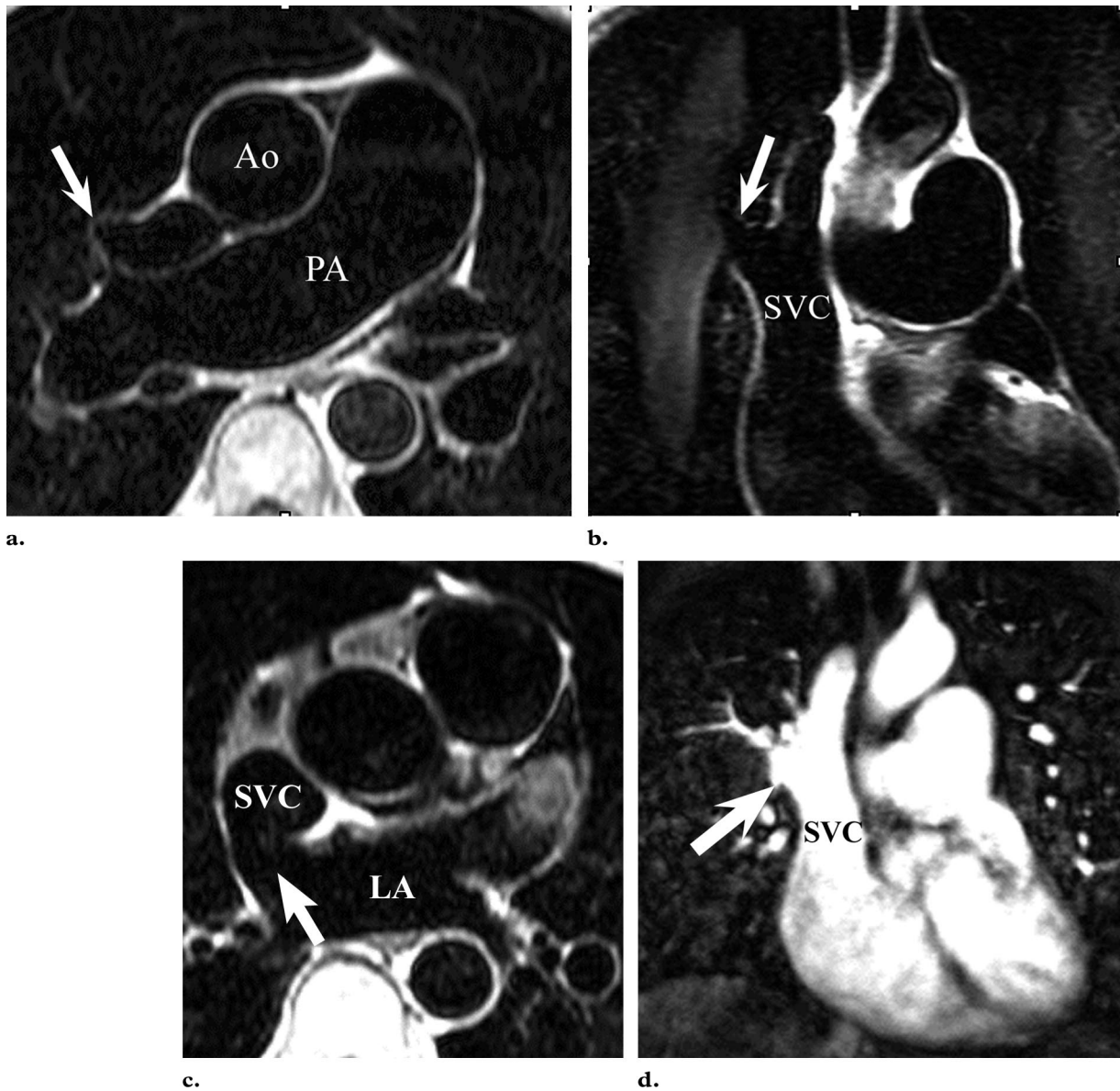
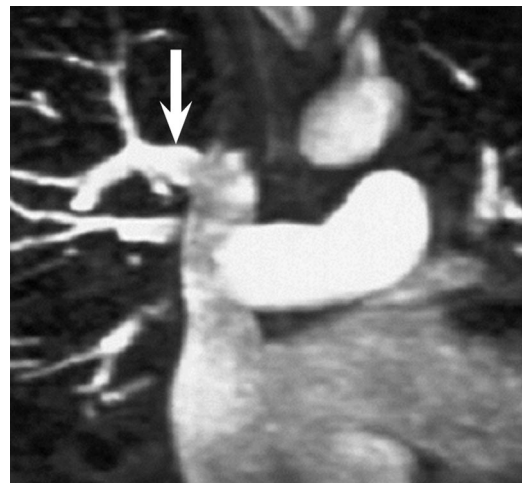


Figure 15. PAPVR in a 71-year-old man with pulmonary arterial hypertension in whom no intracardiac shunt was found at echocardiography. Maximum-intensity projection image from MR angiographic data shows drainage of the right upper lobe pulmonary vein (arrow) into the superior vena cava.



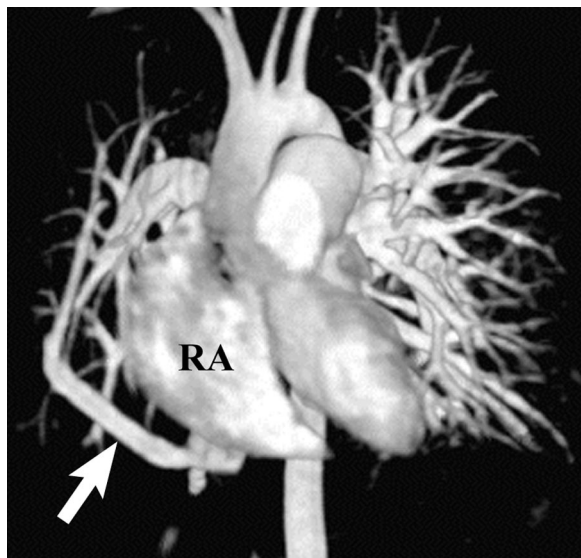


Figure 16. PAPVR in a 45-year-old woman with hypogenetic lung syndrome (scimitar syndrome). Volume-rendered contrast-enhanced MR angiographic image shows drainage of the right upper lobe pulmonary vein (arrow) into the inferior vena cava at its junction with the right atrium (RA). This syndrome involves a combination of various defects, which may include hypoplasia of the right lung and the right pulmonary artery (not shown).

Echocardiography and conventional angiography frequently are used for the diagnosis of PAPVR. Definitive diagnosis, however, may be difficult with echocardiography because of the limited acoustic window, especially in older children and adults (27,28). Although angiography is often considered the standard imaging modality for the diagnosis of anomalous pulmonary veins, it is invasive, and visualization of the veins may be difficult because of the dilution of hand-injected angiographic contrast material. CT, which also has been used to delineate the anatomy in PAPVR (29), requires the use of ionizing radiation and iodinated contrast material.

MR imaging has been used increasingly for the diagnosis of PAPVR because it provides a large field of view and excellent anatomic delineation without contrast material injection or ionizing radiation (Fig 14). MR imaging has been reported to have a greater sensitivity (95%) than do echocardiography (38%) and angiography (69%)



Figure 17. PAPVR in a 43-year-old woman with dyspnea on exertion. Volume-rendered contrast-enhanced MR angiographic image shows drainage of the left upper lobe pulmonary vein (*) into the left vertical vein (+), and eventually into the superior vena cava (●).

in the prospective detection of pulmonary venous anomalies including PAPVR (30). In addition, MR imaging can depict atrial septal defects (13), which are frequently associated with PAPVR (Fig 14c).

MR angiography permits the noninvasive multiplanar assessment of vessel size, course, and location (30). Contrast material-enhanced MR angiography, which provides three-dimensional rapid imaging capability with a large field of view, may demonstrate anomalous drainage patterns more clearly than spin-echo MR techniques (Figs 14d, 15–17). According to a recent report (30), images obtained with contrast-enhanced three-dimensional MR angiography enabled the definitive diagnosis of anomalous pulmonary veins in patients in whom findings at transesophageal echocardiography and cardiac catheterization had been inconclusive.

Table 3
Formulas for Calculating Volume of Cardiovascular Shunts with Cine MR Imaging Techniques

Shunt Type	Cine MR Imaging Volumetrics	Velocity-encoded Cine MR Imaging
Atrial septal defect	Shunt volume = RSV - LSV	Shunt volume = RSV - LSV
Ventricular septal defect	NA*	Shunt volume = RSV - LSV
Patent ductus arteriosus	Shunt volume = LSV - RSV	Shunt volume = LSV - RSV
Aortopulmonary window	Shunt volume = LSV - RSV	Shunt volume = LSV - RSV
PAPVR	Shunt volume = RSV - LSV	Shunt volume = RSV - LSV

Note.—LSV = left ventricular stroke volume, NA = not applicable, RSV = right ventricular stroke volume.

*Quantification of shunt volume in ventricular septal defect is not possible with volumetrics, because the left and right ventricular stroke volumes are equal.

Quantification of Shunts

Measurement of shunt volume is an important aspect of the evaluation of cardiac shunts. Two cine MR imaging methods are available for shunt quantification: the volumetric technique and the flow quantification technique.

The first approach is based on gradient-echo cine imaging in the short-axis plane. The end-diastolic volume (EDV) and end-systolic volume (ESV) are calculated by using a stack of short-axis cine images, and the two values then are summed to obtain the stroke volume (SV), such that $SV = EDV - ESV$. The shunt volume is calculated as the difference between right and left ventricular stroke volumes (Table 3). This method, however, is useless for quantifying the shunt volume in ventricular septal defects, in which the left and right ventricular stroke volumes are equal. Furthermore, the presence of aortic or pulmonic valvular regurgitation may lead to inaccurate determination of stroke volume unless the regurgitation volume is subtracted from the estimated stroke volume.

The second approach involves the use of velocity-encoded cine MR imaging to measure blood flow in the main pulmonary artery (which is equal to the right ventricular stroke volume) and in the

proximal aorta (which is equal to the left ventricular stroke volume) (Fig 18). This phase-contrast sequence is based on the principle that the phase of the spins along a magnetic gradient changes in proportion to flow velocity (31). The shunt volume is the difference between pulmonary arterial flow and aortic flow (Table 3). The accuracy of shunt volume values obtained with the flow quantification method, like those obtained with the volumetric method, may be compromised by valvular regurgitation.

Monitoring of the ratio of pulmonary flow to systemic flow (Fig 19), which indicates the severity of the shunt, can aid in treatment planning. The borderline range is a ratio of 1.7–2.0. Typically, surgery or transcatheter closure is recommended when the ratio exceeds this range (32).

Conclusions

MR imaging is a valuable tool for depicting cardiac anatomy and quantifying function. It is particularly useful for the evaluation of cardiac shunts in supracristal ventricular septal defect, atrioventricular septal defect, and PAPVR, in which echocardiography and conventional angiography have limited use. MR imaging is also well suited for the noninvasive quantification of shunt volume and functional evaluation of shunt severity.

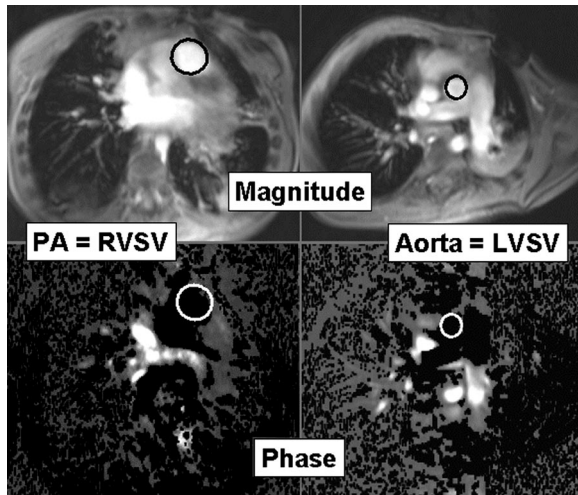


Figure 18. Magnitude (top row) and phase (bottom row) images of the pulmonary artery (left column) and aorta (right column). Flow volume is calculated as the product of the mean flow velocity, which is measured on the phase images, and the cross-sectional area of the vessel. Flow in the pulmonary artery (*PA*) is equivalent to the right ventricular stroke volume (*RVSV*), and flow in the aorta is equivalent to the left ventricular stroke volume (*LVSV*).

References

- Higgins CB, Byrd BF 3rd, Farmer DW, Osaki L, Silverman NH, Cheitlin MD. Magnetic resonance imaging in patients with congenital heart disease. *Circulation* 1984; 70:851–860.
- Higgins CB, Byrd BF 2nd, McNamara MT, et al. Magnetic resonance imaging of the heart: a review of the experience in 172 subjects. *Radiology* 1985; 155:671–679.
- Didier D, Higgins CB, Fisher MR, Osaki L, Silverman NH, Cheitlin MD. Congenital heart disease: gated MR imaging in 72 patients. *Radiology* 1986; 158:227–235.
- Boxt LM. MR imaging of congenital heart disease. *Magn Reson Imaging Clin N Am* 1996; 4:327–359.
- Szolar DH, Sakuma H, Higgins CB. Cardiovascular applications of magnetic resonance flow and velocity measurements. *J Magn Reson Imaging* 1996; 6:78–89.
- Mohiaddin RH, Longmore DB. Functional aspects of cardiovascular nuclear magnetic resonance imaging: techniques and application. *Circulation* 1993; 88:264–281.
- Higgins CB, Sakuma H. Heart disease: functional evaluation with MR imaging. *Radiology* 1996; 199:307–315.

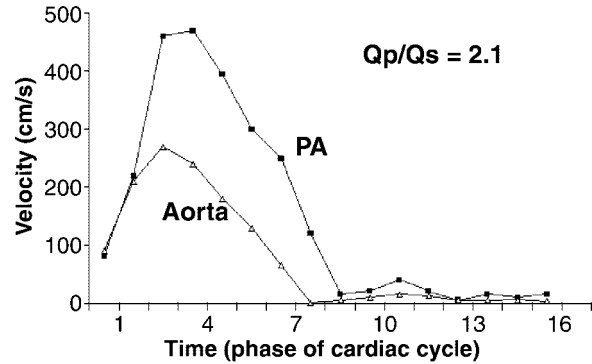


Figure 19. Velocity-versus-time curves for blood flow in the aorta and the pulmonary artery (*PA*). Each point on the curve represents the mean blood flow in the vessel at a particular phase of the cardiac cycle, and each value is derived from a separate velocity-encoded cine MR image. Shunt severity is expressed as the ratio of pulmonary flow (*Q_p*) to systemic flow (*Q_s*).

- Cohen MC, Hartnell GG, Finn JP. Magnetic resonance angiography of congenital pulmonary vein anomalies. *Am Heart J* 1994; 127:954–955.
- Holland GA, Dougherty L, Carpenter JP, et al. Breath-hold ultrafast three-dimensional gadolinium-enhanced MR angiography of the aorta and the renal and other visceral abdominal arteries. *AJR Am J Roentgenol* 1996; 166:971–981.
- Therrien J, Webb GD. Congenital heart disease in adults. In: Braunwald E, ed. *Heart disease: a textbook of cardiovascular medicine*. 6th ed. Philadelphia, Pa: Saunders, 2001; 1592–1621.
- Baron MG. Plain film diagnosis of common cardiac anomalies in the adult. *Radiol Clin North Am* 1999; 37:401–420.
- Kuzman WJ. Atrial septal defects in the older patient: diagnosis and treatment. *Geriatrics* 1967; 22:107–111.
- Diethelm L, Dery R, Lipton MJ, Higgins CB. Atrial-level shunts: sensitivity and specificity of MR in diagnosis. *Radiology* 1987; 162:181–186.
- Higgins CB. Radiography of congenital heart disease. In: Higgins CB, ed. *Essentials of cardiac radiology and imaging*. Philadelphia, Pa: Lippincott, 1992; 49–90.
- Holmvang G, Palacios IF, Vlahakes GJ, et al. Imaging and sizing of atrial septal defects by magnetic resonance. *Circulation* 1995; 92:3473–3480.
- Hundley WG, Li HF, Lange RA, et al. Assessment of left-to-right intracardiac shunting by

- velocity-encoded, phase-difference magnetic resonance imaging: a comparison with oximetric and indicator dilution techniques. *Circulation* 1995; 91:2955–2960.
17. Anderson RH, Lenox CC, Zuberbuhler JR. The morphology of ventricular septal defects. *Perspect Pediatr Pathol* 1984; 8:235–268.
 18. Funabashi N, Rubin GD. Qualitative blood flow differentiation: depiction of a left to right cardiac shunt across a ventricular septal defect using electron-beam computed tomography. *Jpn Circ J* 2000; 64:901–903.
 19. Paul JF, Mace L, Caussin C, et al. Multirow detector computed tomography assessment of intraseptal dissection and ventricular pseudoaneurysm in postinfarction ventricular septal defect. *Circulation* 2001; 104:497–498.
 20. Didier D, Higgins CB. Identification and localization of ventricular septal defect by gated magnetic resonance imaging. *Am J Cardiol* 1986; 57:1363–1368.
 21. Bremerich J, Reddy GP, Higgins CB. MRI of supracristal ventricular septal defects. *J Comput Assist Tomogr* 1999; 23:13–15.
 22. Brenner LD, Caputo GR, Mostbeck G, et al. Quantification of left to right atrial shunts with velocity-encoded cine nuclear magnetic resonance imaging. *J Am Coll Cardiol* 1992; 20:1246–1250.
 23. Parsons JM, Baker EJ, Anderson RH, et al. Morphological evaluation of atrioventricular septal defects by magnetic resonance imaging. *Br Heart J* 1990; 64:138–145.
 24. Studer M, Blackstone EH, Kirklin JW, et al. Determinants of early and late results of repair of atrioventricular septal (canal) defects. *J Thorac Cardiovasc Surg* 1982; 84:523–542.
 25. Garver KA, Hernandez RJ, Vermilion RP, Martin Goble M. Images in cardiovascular medicine: correlative imaging of aortopulmonary window—demonstration with echocardiography, angiography, and MRI. *Circulation* 1997; 96:1036–1037.
 26. Incesu L, Baysal K, Kalayci AG, Erk K. Magnetic resonance imaging of proximal aortopulmonary window. *Clin Imaging* 1998; 22:23–25.
 27. Ammash NM, Seward JB, Warnes CA, Connolly HM, O’Leary PW, Danielson GK. Partial anomalous pulmonary venous connection: diagnosis by transesophageal echocardiography. *J Am Coll Cardiol* 1997; 29:1351–1358.
 28. Seward J. Transesophageal echocardiography. In: Freeman W, Seward J, Khanderia B, Tajik A, eds. *Transesophageal echocardiography*. New York, NY: Little, Brown, 1994; 385–423.
 29. Thorsen MK, Erickson SJ, Mewissen MW, Youker JE. CT and MR imaging of partial anomalous pulmonary venous return to the azygos vein. *J Comput Assist Tomogr* 1990; 14:1007–1009.
 30. Ferrari VA, Scott CH, Holland GA, Axel L, Sutton MS. Ultrafast three-dimensional contrast-enhanced magnetic resonance angiography and imaging in the diagnosis of partial anomalous pulmonary venous drainage. *J Am Coll Cardiol* 2001; 37:1120–1128.
 31. Underwood SR, Firmin DN, Klipstein RH, Rees RS, Longmore DB. Magnetic resonance velocity mapping: clinical application of a new technique. *Br Heart J* 1987; 57:404–412.
 32. Friedman WF, Silverman N. Congenital heart disease in infancy and childhood. In: Braunwald E, ed. *Heart disease: a textbook of cardiovascular medicine*. 6th ed. Philadelphia: Saunders, 2001; 1505–1591.